Structural and Kinetic Molecular Dynamics Study of Electroporation in Cholesterol-Containing Bilayers

M. Laura Fernández,[†] Guillermo Marshall,[†] Francesc Sagués,[‡] and Ramon Reigada*[,‡]

Laboratorio de Sistemas Complejos, Departamento de Computación, Facultad de Ciencias Exactas y Naturales, Universidad de Buenos Aires, 1428 Buenos Aires, Argentina, and Departament de Química Física, Universitat de Barcelona, c/Martí i Franqués 1, Pta 4, 08028 Barcelona, Spain

Received: December 7, 2009; Revised Manuscript Received: March 15, 2010

We present a numerical study of pore formation in lipid bilayers containing cholesterol (Chol) and subjected to a transverse electric field. Molecular dynamics simulations of 1,2-dipalmitoyl-*sn*-glycero-3-phosphatidylcholine (DOPC) membranes reveal the formation of a pore when an electric field of 325 mV/nm is applied. The minimum electric field needed for membrane permeabilization strongly increases with the addition of cholesterol above 10 mol %, reaching 750 mV/nm for 40 mol % Chol. Analysis of simulations of DOPC/Chol bilayers suggests this is caused by a substantial increment of membrane cohesion. Simulations also show that pore formation kinetics is much slower at high Chol contents.

1. Introduction

The cell membrane constitutes the boundary between a cell and its environment, and its structure is determined by the amphiphilic nature of its constituent lipids.[1,2] Membrane lipids self-assemble and orient with their hydrophilic portions facing water, forming a bimolecular layer. This bilayer constitutes a rather impermeable barrier that impedes the passive transport of ions and medium/large molecules across it. Concomitant with the existence of cell-controlled active transport through ion pumps or by more complex endo/exocytosis procedures, passive transport of molecules through the cell membrane is usually mediated by the formation of transient water-filled pores. However, formation of such pores in cell resting conditions has an extremely low occurrence, this being responsible for the low basal ion permeation rates.[3] Reversible pores in cell membranes can be induced by different experimental techniques involving the application of mechanical stress (i.e., micropipet aspiration)[4] or an external electric field. The latter is referred to as electropermeabilization or electroporation[5] and has been used in numerous applications in biotechnology and medicine. For example, it is a common technique for introducing genetic material in cells (RNA transfection, electrogenetherapy),[6,7] and for delivering drugs across the skin[8] and cells.[9] The latter application has resulted in a new tool to battle cancer, electrochemotherapy,[10−12] based on the electroformation of reversible pores in the cell membrane, allowing the delivery of nonpermeant drugs inside tumor cells and enhancing the local cytotoxic effects of these compounds. Such treatments typically consist of the application of pulses of $\sim$100 μs at a field strength of $\sim$1000 V/cm.[10−12]

In addition to experiments, molecular dynamics (MD) simulations are powerful technique for elucidating molecular mechanisms leading to membrane pore formation when a transverse electric field is applied. Following this approach, several works have been devoted to the numerical investigation of electroporation in single-component bilayers, and some molecular details of this phenomenon are being elucidated, at least for simple systems. According to these studies, the disordering of the water−membrane interface due to the applied external field that may eventually generate a water defect initially drives pore formation. Such a water defect can develop into a water column penetrating into the inner region of the bilayer (hydrophobic pore). Further on, the phospholipid head groups reorient to cover the initial water column and form a hydrophilic pore.[13−15] The kinetics of these stages have been characterized.[16,17] Pore collapse leading to membrane reconstitution, when the applied field is removed, has been also described.[16] For asymmetric bilayers in particular, the resealing process after electroporation has been related to experimental observations of phosphatidylserine translocation.[18]

Although MD studies have shed light on the understanding of the molecular mechanism of electroporation, there is an important actor in the cell membrane that has been missing in all these studies: cholesterol. Cholesterol (Chol) is the most common lipid component in animal cell membranes (from 0.1 to 0.4 of molar fraction),[19] and its role is fundamental for explaining many structural properties of the cell membrane. Chol increases the order of fluid-phase phospholipid acyl chains and determines permeability, fluidity, and mechanical properties of membranes.[20] The role of Chol as an agent for promoting membrane order is well established and underlines all the above functions. Most of the physical and functional membrane properties are determined by cholesterol and/or its interaction with the other lipid species. In this context, the understanding of the molecular details of electroporation in mammalian cell membranes requires the study of cholesterol-containing bilayers.

In this work the molecular study of electroporation in bilayers containing different amounts of cholesterol (0, 10, 20, 30, and 40 molar percentage of Chol) is reported, and the particular role of Chol in this phenomenon is analyzed. The numerical study of electroporation of DOPC pure (cholesterol-free) bilayers was presented in the excellent work by Ziegler and Vernier,[14] and here we use their results for comparison with our systems with 0 mol % Chol. Although most of the results are reproduced in our simulations, there are, however, quantitative discrepancies in some particular observables that can be explained as follows.

* Corresponding author. Phone: +34 934039290. Fax: +34 934031231. E-mail: reigada@ub.edu.
[†] Universidad de Buenos Aires.
[‡] Universitat de Barcelona.

10.1021/jp911605b
Published on Web 04/29/2010

DOPC has two monounsaturated acyl tails, and it has been shown that the description of a double bond in a lipid hydrocarbon chain in atomistic MD simulations is a subtle matter.[21] At present, some of the available force fields for lipids (for example the standard GROMOS87 force field[22] used here) parametrize the cis double bond as a simple improper torsion (determining the planarity of the double bond region) together with corrections for the adjacent dihedrals. Recently, by means of ab initio calculations of small molecules like *cis*-2-hexene, Bachar et al.[23] developed another set of force field parameters to describe the double bond region, accounting for *skew* states in the vicinity of the double bond. The new force field has been incorporated by one of us (R.R.) into the description of DOPC bilayers, giving rise to more accurate MD results (for details see refs 21 and 24). In the present work, this improved version of the force field has been used.

One of the main goals of this paper is the calculation of the minimum electroporation field E_0 (namely, the minimum value of the applied electric field that is necessary to induce pore formation) for different cholesterol fractions in tensionless membranes. However, caution must be exercised when the applied fields in our MD simulations are compared with real field values in electroporation experiments. First, the application of periodic boundary conditions and the use of the particle mesh Ewald method to deal with long-range electrostatic interactions may introduce artifacts in the description of the electrostatic charge profiles in MD membrane simulations. Such inaccuracy strongly affects the calculated value for the transmembrane potential in the simulations. Second, it is worth noticing that in the laboratory, the electric field is taken as the potential difference between electrodes divided by the distance separating them. In this regard, it corresponds to the sum of the field due to the free charge at the electrodes and the depolarization field response due to the dielectric nature of the system. In contrast, in our MD simulations, the external applied field, E_{ap}, corresponds to the field generated from the charges at the electrodes without considering the electric response of the dielectric medium. Additional considerations can be found in refs 14 and 17, but they are beyond the scope of this paper. Here, we have chosen the simulated external applied field E_{ap} as a control parameter to compare the electroporating behavior of membranes with different amounts of cholesterol.

2. Methods

2.1. Molecular Dynamics Protocols and Simulations. We carried out atomistic MD simulations of membrane systems composed of DOPC in the fluid phase and different amounts of cholesterol (0, 10, 20, 30, and 40 mol % Chol). The simulations correspond to membranes composed of a total of 128 DOPC molecules (64 at each leaflet) and the corresponding amount of cholesterol molecules (0, 14, 32, 56, and 86, respectively) homogeneously distributed in the two leaflets. All the bilayers are sufficiently hydrated with 6186 water molecules. The systems were constructed from scratch. First, a DOPC system containing 50 mol % cholesterol was constructed by the 4×4 replication of a handmade piece of membrane containing four lipids and four cholesterol molecules in each layer. After 10 ns the equilibrium at 338 K was achieved, and the final configuration was used to construct five membranes with different cholesterol molar percentages after randomly subtracting the corresponding number of cholesterol molecules and preserving an equal amount at each leaflet. Each membrane is brought to equilibrium at 338 K and then cooled for a minimum of 10 ns and a maximum of 20 ns to the working temperature $T = 310$ K. Equilibration of bilayers has been determined by monitoring the membrane area.

Simulations have been performed using the GROMACS software package.[25,26] We have used the standard united-atom force-field parameters,[27] which have been extensively tested and verified. Partial charges were taken from ref 28. For the double bond we used the description by Bachar et al.[23] which explicitly describes the *skew* states of bonds next to the double bond.[21] For cholesterol a description based on that of Holtje et al.[29] has been used. The simple point charge (SPC) model[30] has been used for water.

The simulations were carried out in the *NpT* ensemble (constant particle number, pressure and temperature) at $p = 1$ atm and $T = 310$ K. Temperature and pressure were controlled by using the weak coupling method[31] with the relaxation times set to 0.6 and 1.0 ps, respectively. The temperatures of the solute and solvent were controlled independently, and the pressure coupling was applied separately in the bilayer plane (xy) and the perpendicular direction (z). The SETTLE algorithm[32] was used to preserve the bond lengths in water molecules, whereas the lipid bond lengths were constrained using the LINCS algorithm.[33] A single 1.0 nm cutoff distance was used for the Lennard-Jones interactions. Long-range electrostatic interactions were handled using the particle mesh Ewald method[34] with a real space cutoff of 1.0 nm, β-spline interpolation (of order 6), and direct sum tolerance of 10^{-5}. Periodic boundary conditions with the usual minimum image convention were applied in all three directions, and the time step was set to 2 fs. This simulation protocol has been successfully applied in a large number of previous MD studies, see for instance refs 21, 24, 35, and 36. Molecular visualization was performed using Visual Molecular Dynamics, VMD.[37]

2.2. Measurement of the Minimum Porating Field. The minimum electroporation field, E_0, was computed following a procedure similar to that in ref 14. Each membrane simulation was run independently for 25 ns in triplicate, and a transverse electric field E_{ap} was fixed in the MD simulation protocol. In the case that none of the three replicas of the system displayed pore formation after 25 ns, the field was increased in 25 mV/nm and so on. When at least one of the three replicas was porated, the value of the applied field, E_{ap}, was taken as E_0. Except in the case that the three simulations showed pore formation, a fourth replica was run for the former lower value of E_{ap}. Using this procedure, the values for E_0 at different cholesterol fractions were computed for our simulated membranes (see Table 1 and Figure 1).

At this point it is worth noticing that given the stochastic nature of electroporation, the interpretation of the computed values of E_0 has to be taken with care. As discussed below, water fluctuations at the lipid/water interface are responsible for this phenomenon, and their occurrence depends on the applied field and the structural properties of the membrane. In particular, for a given lipid membrane, if a stronger field is applied, the more often these fluctuations will take place, so that a shorter time will be needed to porate the membrane. Following ref 14, we have performed 25 ns simulations for bilayers of 128 DOPC lipids, and the porating field threshold is computed according to the appearance or absence of pores limited to this time period and bilayer size. These limitations influence the calculation of the values of E_0, and we do not exclude the possibility that smaller values would be obtained if simulations of larger systems and/or to longer times were carried out. The simulations presented here were run for time and bilayer sizes allowed by the available computational resources.

TABLE 1: Membrane Properties[a] and Minimum Electroporating Field

	0 mol % Chol	10 mol % Chol	20 mol % Chol	30 mol % Chol	40 mol % Chol
E_0 (mV/nm)	325	325	475	600	750
A_{DOPC} (Å^2)	71.4/**91.3**	67.2/**87.6**	63.1/**64.1**	59.3/**60.1**	58.2/**58.3**
bilayer thickness (Å)	36.9/**30.3**	38.8/**31.4**	41.7/**40.9**	44.4/**43.3**	44.6/**44.1**
$\langle S_{CD} \rangle$	0.098/**0.040**	0.125/**0.056**	0.149/**0.145**	0.191/**0.190**	0.223/**0.212**
⟨PN angle⟩ (deg)	77.39	77.56	78.64	79.09	79.04
⟨PN angle cathode/anode⟩ (deg)	**69.15/79.20**	**70.20/80.75**	**72.27/82.02**	**72.57/85.97**	**72.53/85.45**

[a] When two numbers share a table cell, normal letters are used for the systems with $E_{ap} = 0$, whereas **bold letters** are used for the systems with $E_{ap} = E_0$. In the latter case, the temporal average is performed when the measured property reaches its stationary value and before the pore appears.

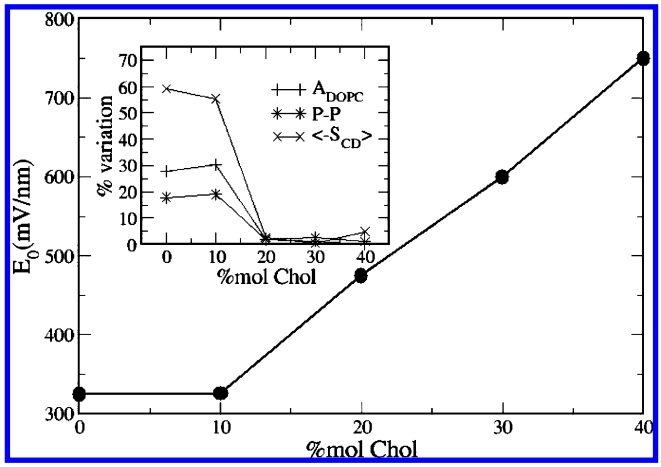

Figure 1. Minimum electroporation field E_0 plotted for different molar % of cholesterol in DOPC membranes at 310 K. The inset shows the % of variation of several structural membrane properties due to the applied electric field $E_{ap} = E_0$. A sharp increment of the membrane cohesion is found above 10 mol % Chol.

In any case, the values of the minimum applied electric field presented here for different membrane compositions are reliable enough to be used for comparative purposes.

The randomness of the poration process is clearly observed in Table 2 where the poration times for different simulations are presented. The poration time corresponds to the time needed to start the generation of the hydrophobic pore in the bilayer once the electric field is applied. In practice, the formation of the hydrophobic pore causes a sudden increase of the total membrane area that we used to determine the electroporation time. In general, when a stronger electric field above E_0 is applied, a shorter time is needed to observe the onset of the first pore in the bilayer. However, this is only true in a statistical sense, since the individual simulations may display results with statistical dispersion. For instance, one simulation for 20 mol % Chol with $E_{ap} = 475$ mV/nm led to pore onset after 8.8 ns, whereas other simulations with the same composition and a larger $E_{ap} = 525$ mV/nm resulted in pores at longer times (14.6, 22.9 ns) or did not even show pore formation after 25 ns. Poration times for several values of applied electric fields are presented in Table 2 for each membrane composition to illustrate the stochastic nature of electroporation.

2.3. Measurement of Membrane Properties. In Table 1, some representative membrane structural properties computed in two different conditions have been summarized. We focused on four membrane structural properties (bilayer thickness, area per lipid, acyl tail ordering, and headgroup orientation) and several bilayer transverse profiles. First, the property was measured when no electric field is applied. Second, the same membrane variable of interest was computed when $E_{ap} = E_0$ and before a pore was formed. In all cases, statistics over 1 ns of each simulation was performed.

TABLE 2: Poration Times[a] for Simulation Replicas at Different % mol Chol

E_{ap} (mV/nm)	poration time (ns)		
	0 mol % Chol		
325 (E_0)	10.5	–	–
350	5.0	7.0	11.8
375	0.7	1.9	6.4
	10 mol % Chol		
325 (E_0)	15.0	–	–
350	6.0	13.0	–
375	11.6	12.8	16.2
	20 mol % Chol		
475 (E_0)	8.8	–	–
525	14.6	22.9	–
575	2.1	2.2	12.2
	30 mol % Chol		
600 (E_0)	17.2	24.4	–
650	4.3	4.5	17.1
700	1.9	2.9	9.6
	40 mol % Chol		
750 (E_0)	8.8	18.8	–
800	8.2	9.0	20.8
850	4.5	9.0	9.0

[a] Dashed symbol means that no pore has been formed in the simulated membrane after 25 ns.

The average area per DOPC molecule, A_{DOPC}, can be calculated in a single-component system by dividing the total average area of the membrane, A, by the number of DOPC molecules in a single leaflet ($N_{DOPC} = 64$). For bilayers with cholesterol, the determination of A_{DOPC} is not obvious since there is no unique way to decompose the cross-sectional area between the two components. The Hofsäß et al.[38] procedure was followed, where the area per PC is defined as

$$A_{DOPC} = \left(\frac{A}{N_{DOPC}}\right)\left(1 - \frac{N_{chol}V_{chol}}{V - N_w V_w}\right)$$

Here V is the volume of the simulation box, N_{DOPC} is the number of DOPC molecules in a leaflet, N_w is the number of water molecules, V_w corresponds to the volume occupied by a water molecule, N_{chol} stands for the number of cholesterols in the membrane, and V_{chol} is the volume of a cholesterol molecule. The value $V_w = 309$ Å^3 was obtained from an independent simulation of a slab of 4142 water molecules under identical simulation conditions, and the volume occupied by a cholesterol molecule was taken to be 541 Å^3.[39]

The bilayer thickness was measured as the average distance between the phosphorus atoms in the opposite leaflets, hereafter referred also as the P−P distance.

To quantify the ordering of DOPC acyl chains, the deuterium order parameter,[40] S_{CD}, profiles along the chains were computed. S_{CD} is defined as

$$S_{CD} = \frac{1}{2}\langle 3\cos^2\theta - 1\rangle$$

where θ is the angle between the carbon−deuterium (CD) bond and the bilayer normal. The angular brackets denote averaging over time and over all CD bonds in a given carbon position. Following the usual practice in united-atom simulations, deuterium positions were constructed from neighboring carbons assuming ideal geometries (taking into account carbon segments connected by a single or a double bond). Larger values for $-S_{CD}$ imply higher chain ordering. Once the deuterium order parameter was computed for all tail carbon groups, the global acyl tail order was taken as the average $\langle S_{CD}\rangle$ for all CD bonds.

The behavior of the DOPC molecules at the lipid/water interface was addressed by analyzing the vector connecting the phosphorus and nitrogen atoms in the headgroup, hereafter referred to as PN vector. The distribution of the angle between the PN vector and the bilayer normal (pointing outward in both leaflets) was computed for the cases with and without applied field. When the field was applied, the two leaflets were not equivalent any more, and the PN distributions were computed separately for the anode and cathode leaflets. From each distribution, the average PN angle was calculated.

Finally, the study of the transverse structure of the membrane system was addressed by computing several averaged properties as a function of the "z"-axis ("z"-profiles). Mass density for different molecules and/or lipid groups provides the information of the distribution of the system components in the "z"-coordinate. The orientation of water molecules close to the lipid/water interface was analyzed with the profiles of the "z"-projection (μ_z) of the water dipole moment ($\vec{\mu}$). The effect of the applied field on the profiles of the electric field (E) due to the charges of different systems components was also analyzed. All the "z"-profiles presented in this paper, were plotted as a function of a rescaled "z"-axis (Z') in such a way that the average location of phosphate groups at each leaflet were placed at $Z' = \pm 1$. Although different simulation conditions altered the bilayer thickness, this effect is already reported in the table containing the P−P distances. So, the definition of the Z' scale in the presented profiles allows a comparison between different profiles separately from the effects due to the change in bilayer thickness.

3. Results and Discussion

3.1. Minimum Porating Field. The poration threshold field obtained for our pure DOPC bilayers is $E_0 = 325$ mV/nm, significantly smaller than in Ziegler and Vernier (380 mV/nm).[14] The reason for this quantitative discrepancy is found in the used MD force field. As previously mentioned, the original standard GROMOS87 force field[22] incorrectly parametrizes the cis double bond[21,23] of the DOPC molecule. In our simulations a corrected and tested[21] double bond parametrization has been used, resulting in bilayers larger and thinner than those obtained with the original force field. Consequently, when the external electric field is applied, the occurrence of water defects capable of penetrating the membrane increases (see below), and therefore a lower value for E_0 is obtained in relation to the simulations performed by Ziegler and Vernier. Some results from simulations using the standard GROMOS87 force field are available as Supporting Information. In any case, the comparison between our structural parameters and the experimental data shows a good agreement. For example, X-ray observations for fully hydrated DOPC bilayers at 303 K provide the range 72.1−72.5 Å^2 for the area per lipid[41,42] (71.4 Å^2 in our simulations). The thickness of pure DOPC bilayers is obtained experimentally from the phosphorus peaks in electron density profiles at 303 K leading to the range 36.7−37.1 Å,[41,42] while we found a value of 36.9 Å.

When cholesterol was added to the bilayer above 10 mol %, stronger electric fields were needed to porate our simulated membranes. The main observation is that the larger the fraction of cholesterol in the bilayer, the higher electroporation field threshold E_0 obtained (see Table 1 and Figure 1). This finding is in agreement with experimental observations of electroporation of cholesterol-containing bilayers. Needham and Hochmuth[43] performed permeabilization of stearoyloleylphosphatidylcholine (SOPC) and SOPC/Chol bilayers by means of electromechanical techniques, namely, by applying voltages to vesicles suctioned in a micropipet setup. One of the main results of this work is that for membranes under zero mechanical tension the permeabilization (poration) voltage was found to increase with increasing cholesterol contents. More recently, Koronkiewicz and Kalinowski[44] performed chronopotentiometric studies with egg yolk phosphatidylcholine planar bilayers with and without cholesterol. The application of a constant current intensity through these bilayers generated pores, and the presence of cholesterol was found to increase the value of the breakdown potential. Recently, MD simulations for dipalmitoylphosphatidylcholine (DPPC) bilayers have demonstrated that addition of cholesterol increases the free energy barrier for transferring DPPC head groups to the center of the bilayer, resulting in a dramatic slowing down of lipid flip-flop events in cholesterol-containing membranes.[45] This finding also suggests a greater difficulty to form pores at high cholesterol contents, in agreement with our results.

3.2. Membrane Structural Properties. Addition of cholesterol to lipid membranes is known to alter their structural properties. The main attribute that makes cholesterol a unique lipid molecule is its ability to condense fluid lipid bilayers.[46] Such a condensing effect can be observed experimentally in several membrane properties, for instance, as a decrease of the area per molecule and an increment of bilayer thickness and acyl chain ordering, These condensing effects have been captured in our simulations.

The thermodynamic origin of the condensing effect of cholesterol is based on its nonideal mixing behavior with the other lipids in the membrane. Cholesterol causes the area per lipid, A_{DOPC}, to decrease with the cholesterol fraction. Table 1 presents the measured values for A_{DOPC} in the simulated membranes without an applied electric field. As the cholesterol contents increases, the area per lipid becomes progressively smaller than for the single-component membrane. As expected, a decrease in area per lipid is accompanied by an increase of the bilayer thickness. In Table 1, the P−P distances for different cholesterol fractions are presented. The values for area per lipid and membrane thickness obtained from our simulations are also in a good agreement with experimental observations in cholesterol-containing membranes. For example, experimental measures for DOPC bilayers with molar 20% cholesterol lead to $A_{DOPC} = 67.3-67.5$ Å^2 and a P−P distance of 39.5 Å,[41,42,46] whereas we obtain $A_{DOPC} = 63.1$ Å^2 and P−P distance equal to 41.7 Å in our simulations for $E_{ap} = 0$. For both variables a reasonable error of 6−7% is found relative to the experimental data. For more details and a deeper discussion on the comparison

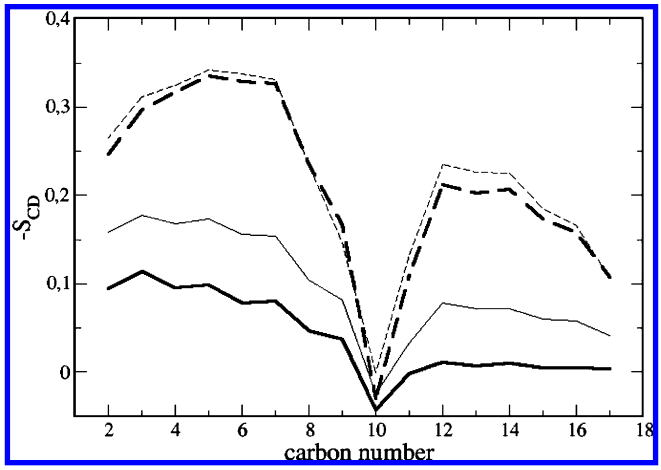

Figure 2. Deuterium order parameter S_{CD} profiles of the *sn*-1 chain of DOPC molecules in a pure bilayer (solid lines) and bilayers with 40 mol % Chol (dashed lines). Thin lines correspond to systems without an applied field whereas thick profiles correspond to the cases where E_0 is applied and the pore is still not formed. The double bond in DOPC molecules is placed between carbons 9 and 10.

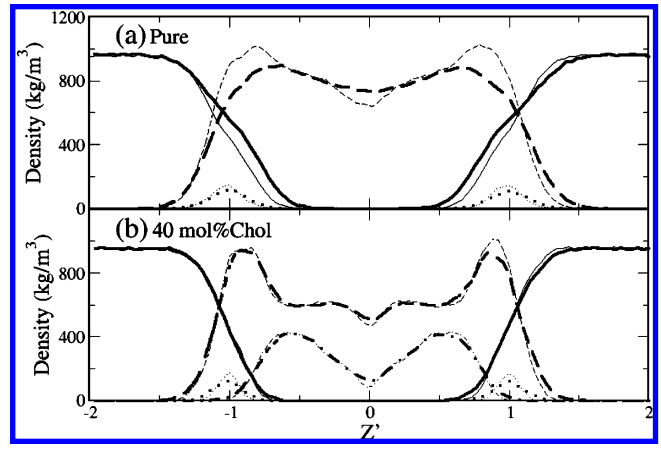

Figure 3. Density profiles are plotted for lipids (dashed), water (solid), and cholesterol (dot-dashed) if present. For the simulations without an applied electric field (thin lines), the average of the last nanosecond of thermalization is performed. When applied, the simulated electric field corresponds to E_0 (thick lines), and in this case the average is performed for 1 ns once the area reaches its stationary state but before the pore is formed. Since the bilayers become thinner when the electric field is applied, the *z*-axis has been rescaled (Z') in such a way the phosphate maxima (dotted) are placed at $+1$, -1, to facilitate the comparison between the cases with and without field. (a) Pure DOPC bilayers. (b) DOPC bilayers with 40 mol % Chol.

of our simulations of cholesterol-containing bilayers to experimental data see refs 21 and 24.

The molecular mechanism that leads to membrane condensation is mostly related to the ordering ability of cholesterol. Placed between lipid molecules, the sterol rigid structure orders the surrounding lipid acyl chains. The deuterium order parameter profiles for the *sn*-1 chains of DOPC for a pure and a 40 mol % Chol membrane, both at $E_{ap} = 0$ and $E_{ap} = E_0$, are shown in solid lines in Figure 2. In all the profiles, a dip at the carbon segments involved in the double bond is clearly noticed, as observed in a number of experimental studies. The comparison of the two cases at $E_{ap} = 0$ shows a substantial increase of the profiles when cholesterol is added, meaning that it strongly orders the DOPC acyl chains. In both cases, when an electric field is applied, lipid acyl chains become more disordered, and this effect is more relevant for pure bilayers. The values for the averaged tail order $\langle S_{CD} \rangle$ reported in Table 1 display, as expected, an increasing behavior with the cholesterol contents.

The insertion of water and cholesterol in the membrane is crucial in electroporation and they can be studied by examining the density "*z*"-profiles. In Figure 3 the profiles for the pure (panel a) and the 40 mol % Chol (panel b) are plotted for different molecules and atom groups of the system. Notice from this figure that water significantly penetrates the headgroup region of the membrane only in the pure system. As observed in diffraction experiments, the lipid density in the region where cholesterol resides is reduced and a plateau appears. More importantly, cholesterol is found to reside in a deeper (more hydrophobic) region of the bilayer than the DOPC head groups (compare the peaks corresponding to cholesterol molecules and phosphate groups in Figure 3b). This fact is important when the molecular sequence of pore formation in cholesterol-containing membranes is analyzed (see below). When the electric field is applied, density profiles are not altered except that water insertion is found to be greatly enhanced for the pure bilayer. This effect is almost imperceptible in the 40 mol % Chol case (see Figure 3). As it will be reported below, the behavior of these water molecules is the determinant for the electroporation process.

A clear correlation is found between the behavior of the structural properties discussed so far and the dependence of E_0 with cholesterol fraction (see Table 1). Membranes with smaller area per lipid and more ordered and packed acyl chains require stronger electric fields to be electroporated. From a mechanistic point of view it is clear that pore formation would be more unlikely in thicker and more densely packed membranes. The cholesterol condensing effect acts, therefore, against pore electroformation. Actually, spontaneous permeation is known to be strongly reduced in a lipid membrane upon addition of cholesterol,[47,48] so an analogous effect is found here for electroporation.

Despite the connection reported above, membranes made of different lipid components but displaying similar structural values for area per lipid, thickness, and chain ordering may show distinct values for E_0. So, instead of these structural variables, electroporation occurrence is generally related to another bilayer property: the area expansivity. The area expansivity modulus of a membrane corresponds to the free energy variation relative to the variation of membrane area under dilation (or condensation) in the absence of bending and shear modes,[49,50] and it accounts for the cohesive nature of the membrane. Experimental studies clearly show how addition of cholesterol into a lipid membrane increases its cohesion, and this effect is generally expressed by an electromechanical rupture of the membrane at larger critical voltages.[43,44,50]

Our numerical simulations do not provide a direct measure of the area expansivity modulus of the simulated membranes. However, we take advantage of the effects of the applied electric field on the membrane properties to indirectly make a qualitative estimation of its behavior. In the context of lipid bilayers subjected to electric fields, it is known that the applied field induces a compressive stress perpendicular (and inward) to the bilayer surface that results in membrane expansion.[43,49] The response (expansion) of the membrane once the electric field is applied depends on the membrane expansivity modulus; namely, on its cohesive nature. We are able to estimate this effect by looking, for example, at the A_{DOPC}, the P−P distance, and the $\langle S_{CD} \rangle$ values once the membranes are adapted to the applied field. These values are presented in Table 1 and in the inset of Figure 1 for membranes subjected to $E_{ap} = E_0$. The response of cholesterol-free bilayers to E_{ap} is significant, with an increment

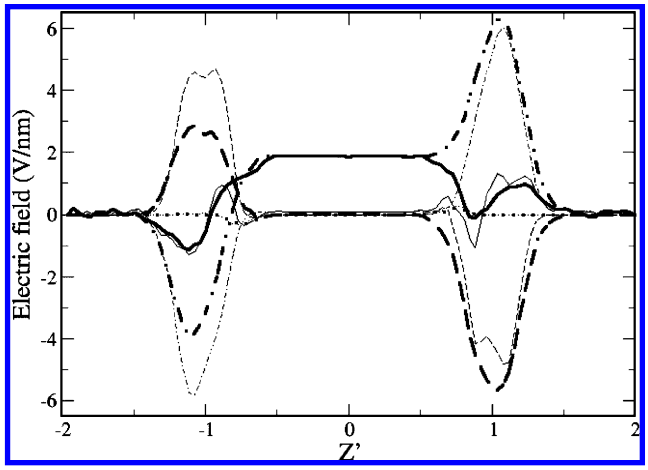

Figure 4. Electric field profiles for DOPC bilayers with 40 mol % Chol. The different curves correspond to the electric field due to the whole system components (solid), lipids (dashed), water (dot-dashed), and cholesterol (dotted). For the simulation without an applied electric field (thin lines), the average of the last nanosecond of thermalization is performed. When applied, the simulated electric field corresponds to E_0 (thick lines), and in this case the average is performed for 1 ns once the area reaches its stationary state but before the pore is formed. As in previous profile figures, the z-axis has been rescaled (Z') in such a way the phosphate density maxima are placed at $+1$, -1.

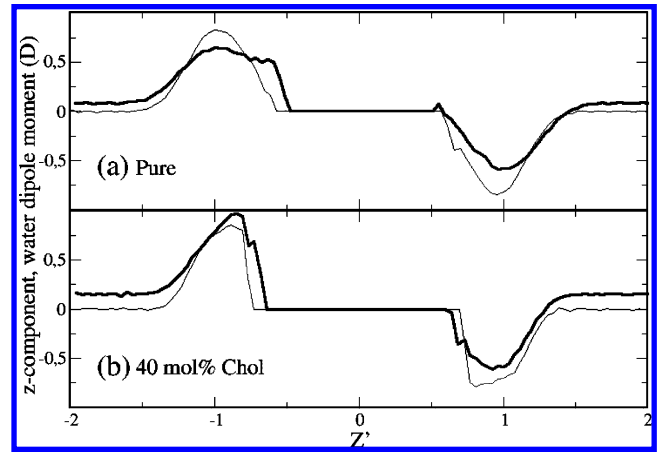

Figure 5. Averaged profile of the z-component of the water dipole moment, μ_z. For the simulations without an applied electric field (thin lines), the average of the last nanosecond of thermalization is performed. When applied, the simulated electric field corresponds to E_0 (thick lines), and in this case the average is performed for 1 ns once the area reaches its stationary state but before the pore is formed. As in previous profile figures, the z-axis has been rescaled (Z') in such a way the phosphate density maxima are placed at $+1$, -1. (a) Pure DOPC bilayers. (b) DOPC bilayers with 40 mol % Chol.

of A_{DOPC} of 28% and a reduction of the bilayer thickness and average ordering parameter of 18% and 59%, respectively. For membranes with 10 mol % Chol, these variations are slightly increased. However, above 10 mol % Chol, the expansive effect of the applied field is sharply reduced to insignificant variations. For example, membranes containing 40 mol % Chol show a rather irrelevant variation of membrane area and thickness smaller than 2%. This finding evidences a sudden increase of the membrane cohesion above 10 mol % Chol that agrees with the sharp increase of E_0 between the 10 and 20 mol % Chol cases. This jump is important in the biological context since cholesterol contents in mammalian plasma membranes are know to be higher than 20 mol %.[51]

3.3. Water and Lipid Headgroup Dipoles. Besides the explanation in terms of global membrane properties, an understanding of the detailed molecular mechanism of electroporation is attempted by analyzing the behavior of the lipid/water interface. First, the "z"-profiles for the different electric field contributions (due to the different components) were examined. In Figure 4 these profiles are plotted for the case of 40 mol % Chol. In the absence of an applied field, the membrane interior has a zero electric field since water and lipids (both DOPC and Chol) balance their dipoles at each leaflet interface region. When an external field is applied, water dipoles at opposite leaflets do not balance any more and the membrane interior has a positive electric field. This means that water molecules orient in a particular manner at the lipid/water interfaces in response to the applied electric field. We notice that the qualitative observations discussed for Figure 4 are common to other cholesterol fractions and even for the pure DOPC bilayers. Actually, cholesterol has little influence in the membrane electric field profiles (see dotted curves in Figure 4).

The behavior of water orientation at the membrane interfaces is characterized by the profiles of the "z"-component of the water dipole moment, μ_z. In Figure 5 these profiles are plotted for the pure bilayer (panel a) and for the 40 mol % Chol system (panel b), in both cases for $E_{ap} = 0$ and $E_{ap} = E_0$. In the absence of an applied field, water dipoles at the two leaflet interfaces point to opposite directions but in a rather symmetrical manner, thus explaining the cancellation of the water contribution to the electric field observed in the dot-dashed thick curve of Figure 4. Water molecules are rather ordered at the water/lipid interface with their hydrogen atoms pointing to the membrane interior, so that the formation of hydrogen bonds with the lipid head groups is maximized. When an external field is applied, the latter configuration is reinforced at the anodic leaflet ($Z' < 0$) but randomized at the cathodic interface ($Z' > 0$), since water at this leaflet is forced to reverse its orientation according to the applied field. Such asymmetry is observed in Figure 5, and it is more evident for the cholesterol-containing system since the applied field is stronger in this case.

The force exerted in the "z"-direction on water molecules due to the electric field gradient is given by $F_z = \mu_z(\vec{\nabla}E)_z$, where $(\vec{\nabla}E)_z$is the "z"-component of the electric field gradient. Simplifying the information in Figure 4, the total electric field vanishes far from the membrane and reaches a rather constant positive value in the bilayer interior, so that its gradient $(\vec{\nabla}E)_z$ is positive in the anodic interface and negative in the cathodic interface. As a consequence, those water molecules at the cathodic water/lipid interface that have reversed their dipole following the external electric field ($\mu_z > 0$) are forced to move to the membrane interior ($F_z < 0$). These molecules may be responsible for the initiation of a thin water hole penetrating the membrane hydrophobic region. Actually, in our MD simulations the formation of water fluctuations (defects) is visually identified at both sides of the membranes, though more often at the cathodic interface (see below). These water fluctuations may either evolve until the full pore is formed or retract after some time, recovering the initial configuration. In fact, all fully completed pore events that have been characterized in our simulations are initiated at the cathodic side.

Another factor that may affect the occurrence of pore electroformation is related to the behavior of lipid headgroup dipoles. The distributions of PN angles (angle between the PN vector and the bilayer normal) have been computed in our simulations (see Figure 6 for the pure and 40 mol % Chol systems at $E_{ap} = 0$ and $E_{ap} = E_0$), and their average angle values are presented (see Table 1). First, we compare the averages for different amounts of cholesterol in the absence of an applied

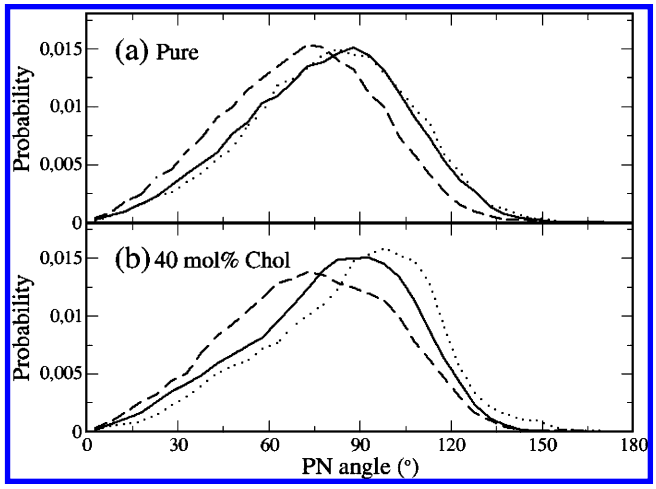

Figure 6. Probability distributions of the angle between the PN vector and the bilayer normal. For the simulations without an applied electric field (solid), the average on the two layers in the last nanosecond of thermalization is performed. When applied, the simulated electric field is E_0, and in this case the average is performed separately for the cathodic (dashed) and anodic (dotted) layers for 1 ns once the area reaches its stationary state but before the pore is formed. (a) Pure DOPC bilayers. (b) DOPC bilayers with 40 mol % Chol.

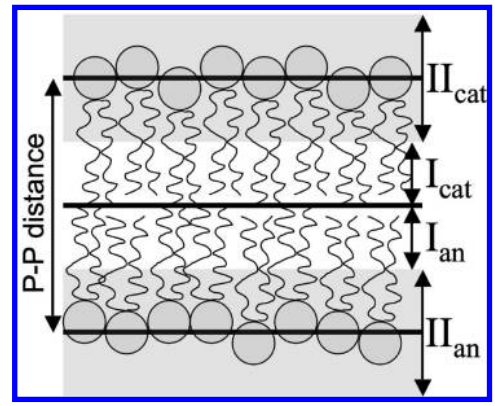

Figure 7. Schematic representation of the four membrane slices in the normal direction (z-sectors) that are used to study pore formation dynamics. Once the P−P distance is determined, the membrane can be divided into two anodic and two cathodic sectors. Each sector I (I_{cat} and I_{an}) corresponds to the 25% of the inner part of the membrane, and each sector II (II_{cat} and II_{an}) comprises the lipid−water interface.

field. In all cases the head groups are pointing almost parallel to the bilayer surface, with a small deviation to the water medium. The presence of cholesterol makes the PC head groups more parallel to the membrane plane and slightly increases the angle average relative to the pure system (Table 1). Two different cholesterol effects for the PC head orientation are found in the literature. On the one hand, cholesterol decreases the area per molecule, and this forces the PC head groups to turn to the water phase (this is found in MD simulations for DMPC/Chol bilayers[52]). On the other hand, interaction with the cholesterol hydroxyl groups orientates the PC head groups toward the bilayer center (as it happens for DPPC/Chol bilayers[53]). In our systems, the latter effect dominates.

When the electric field is applied, head groups at the cathodic and anodic membrane interfaces behave differently. PN vectors try to be aligned with the external applied field, so that they shift to smaller angles (outward) at the cathodic side and to larger angles (inward) at the anodic leaflet (see Figure 6). The averages of the PN angles in the two leaflets can be compared in Table 1, and the observed differences are 8−12° without any clear dependence on the cholesterol content in the membrane. Although the differences found here are larger than those observed for DOPC membranes in ref 14 (6°), we also support the idea reported by Ziegler and Vernier that the headgroup orientation is not the determinant causative factor in electroporation (at least compared to the effect of the water orientation at the lipid/water interface and the cohesive nature of the membrane, as discussed so far). A detailed discussion on this issue can be found in ref 54. In any case, the large increment of E_0 upon addition of cholesterol reported here is definitely not due to the variations showed for the lipid headgroup orientations at both leaflets.

3.4. Kinetics of Pore Formation. The direct observation of the dynamic sequence of pore formation reveals the molecular mechanism of the electroporation process. The complete sequence of pore formation can be described as follows. First, a group of dipole-aligned water molecules forms a water fluctuation or defect that slightly penetrates the hydrophobic region of the membrane. Second, this water defect forms a very thin cone of water molecules that approaches the bilayer center. Third, this water intrusion progresses and may eventually reach the opposite leaflet, forming a thin hydrophobic water pore. We notice that all the visualized pores in our simulations originate in the cathodic leaflet. We also show that during the pore onset the anodic interface is not perturbed until the complete hydrophobic pore is formed. Moreover, it can be observed that water molecules forming the pore have their dipoles oriented according to the external field. In a fourth stage, the lipids around the pore rotate and cover the water filament with their hydrophilic head groups, forming a hydrophilic pore that rapidly widens. This sequence is common to all our simulated bilayers and it is also similar to the mechanisms reported in other MD studies of membrane electroporation.[13,14,16,17]

However, some distinct features between cholesterol-free and cholesterol-containing membranes are observed in the electroporation process. These differential features are connected to the different kinetic behavior of the system components in the pore formation sequence. The quantitative study of the kinetics of the electroporation molecular mechanism is performed by computing the temporal evolution of the number of particular atoms or groups (water molecules, phosphate groups of DOPC, and hydroxyl groups of Chol) residing in different regions of the membrane system. For this purpose, the membrane is divided in four slices in the "xy" plane ("z"-sectors). Regions I correspond to most inner sections that comprise all atoms with "z"-coordinate $\in (Z_{med}, Z_{med} \pm 0.25Z_{P-P})$, where Z_{med} is the "z" value of the center of the bilayer and Z_{P-P} is the P−P distance. Regions II contain the more external part of the membrane with $z \in (Z_{P,i} - 0.25Z_{P-P}, Z_{P,i} + 0.25Z_{P-P})$ where $Z_{P,i}$ is the "z"-coordinate of the center of the phosphorus groups in the leaflet "i". Each region may correspond to the cathodic (I_{cat}, II_{cat}) or to the anodic leaflet (I_{an}, II_{an}). A schematic representation of this partitioning is depicted in Figure 7.

Representative temporal evolution of the number of water molecules and phosphate groups of a pure DOPC membrane at $E_{ap} = E_0 = 325$ mV/nm are plotted in Figure 8 for the four "z"-sectors. The sudden increase of water molecules in the inner sectors ($I_{cat,an}$) after $t = 9500$ ps indicates the starting point of pore formation in this particular simulation. The jump of water molecules in the I_{cat} region is immediately followed by the jump in I_{an}, meaning that water molecules traverse fast the bilayer and the hydrophobic pore is formed very quickly. Rotation of DOPC lipids to form the hydrophilic pore takes place in few

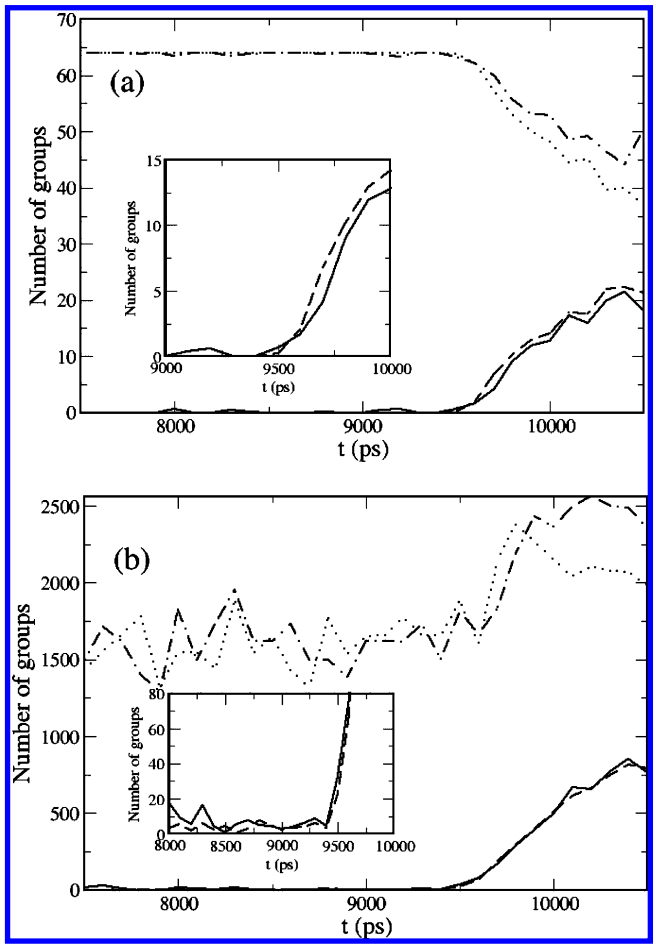

Figure 8. Temporal evolution of the number of groups in different z-sectors of a pure DOPC membrane subjected to an applied electric field $E_{ap} = E_0 = 325$ mV/nm and showing pore formation. In (a) phosphate groups and in (b) water molecules are analyzed. The line texture corresponds to the analyzed z-sector (Figure 7): dotted (II_{an}), dashed (I_{an}), solid (I_{cat}), and dot-dashed (II_{cat}). A smaller scale in the y-axis is used in the insets to look in more detail the behavior in the $I_{cat,an}$ sectors. The pore is formed very quickly at $t = 9500$ ps. Water rapidly traverses the membrane and forces the DOPC lipids to rotate and form the hydrophilic pore in a few tens of picoseconds. Molecular plots of the different stages of pore formation for this case are presented in Figure 10.

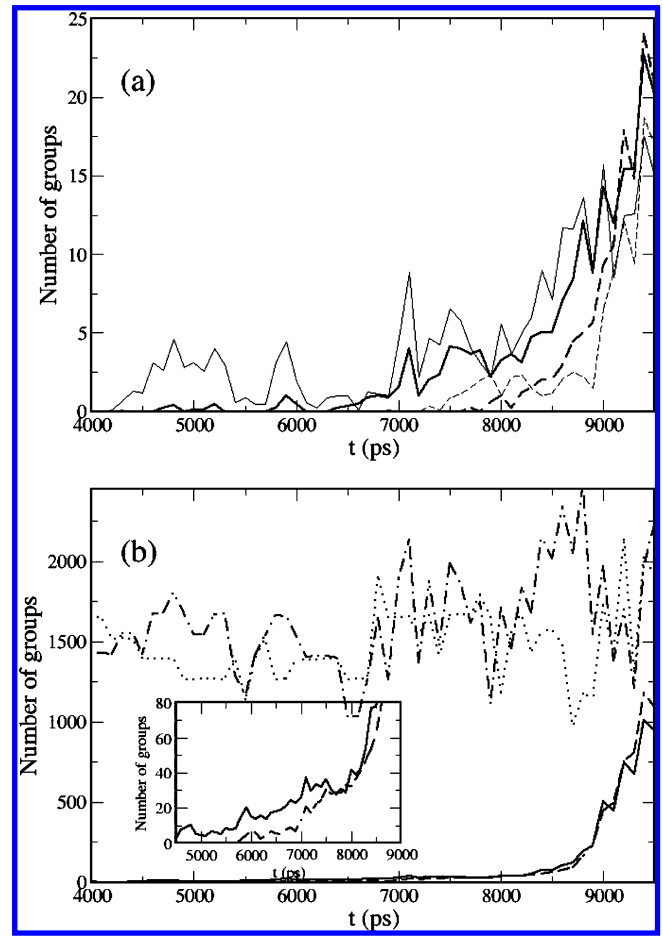

Figure 9. Temporal evolution of the number of groups in different z-sectors of a DOPC bilayer with 40 mol % Chol, subjected to an applied electric field $E_{ap} = E_0 = 750$ mV/nm and showing pore formation. In (a) phosphate (thick lines) and cholesterol hydroxyl (thin lines) groups and in (b) water molecules are analyzed. The line texture corresponds to the analyzed z-sector (see Figure 7): dotted (II_{an}), dashed (I_{an}), solid (I_{cat}), and dot-dashed (II_{cat}). For clarity, sectors II have not been plotted in (a). A smaller scale in the y-axis is used in the inset of (b) to look in more detail the behavior of water in the $I_{cat,an}$ sectors. The pore is formed very slowly starting at $t = 4500$ ps with an initial water fluctuation that persists and traverses the membrane after 2−3 ns. First, Chol molecules and a little later DOPC lipids, rotate and form the hydrophilic pore. Molecular plots of the different stages of pore formation for this case are presented in Figure 11.

tens of picoseconds as it is observed in the tiny delay between the jump of water and phosphates in regions I. Molecular plots of the different stages of pore formation for this case are presented in Figure 10.

Representative temporal evolution of the number of water molecules, phosphate and Chol hydroxyl groups of a DOPC membrane with 40 mol % Chol at $E_{ap} = E_0 = 750$ mV/nm are plotted in Figure 9 for the four "z"-sectors. In this particular simulation, the pore seems to be initiated around $t = 5000$ ps since a sustained growth of water molecules in the I_{cat} region is observed. For a long period (about 2 ns) the water defect tries to traverse the membrane and, at about $t = 7000$ ps, the sector I_{an} starts to be filled with water molecules. After this, it can be observed that Chol fills the inner sectors of the membrane about 0.5−1 ns before DOPC molecules. This means that the rotation of Chol molecules appears to be faster than DOPC rotation, and this is probably due to the fact that Chol hydroxyl groups are inserted deeper into the membrane than DOPC head groups. In any case, rotation of lipids results in the hydrophilic pore after several hundreds of picoseconds. Molecular plots of the different stages of pore formation for this case are presented in Figure 11.

The distinct features in the kinetics of the electroporation process observed when cholesterol-free and cholesterol-containing membranes are compared can be visualized by means of MD snapshots (Figures 10 and 11) and are summarized as follows. In the absence of cholesterol, the occurrence of water fluctuations is much higher (compare Figures 10b and 11b). Once a fluctuation penetrates sufficiently into the membrane, the hydrophobic pore is formed almost simultaneously (snapshots in Figure 10b,c are only separated by 30 ps). The hydrophobic pore only lasts a few hundreds of picoseconds since DOPC molecules quickly rotate to stabilize the hydrophilic pore (the time period between snapshots in Figure 10c,d is only 200 ps). Instead, for cholesterol-containing membranes, pores are formed following a much slower kinetics. In these cases, water fluctuations are less probable than for the pure system. Once a water defect is formed, traversing the membrane and connecting

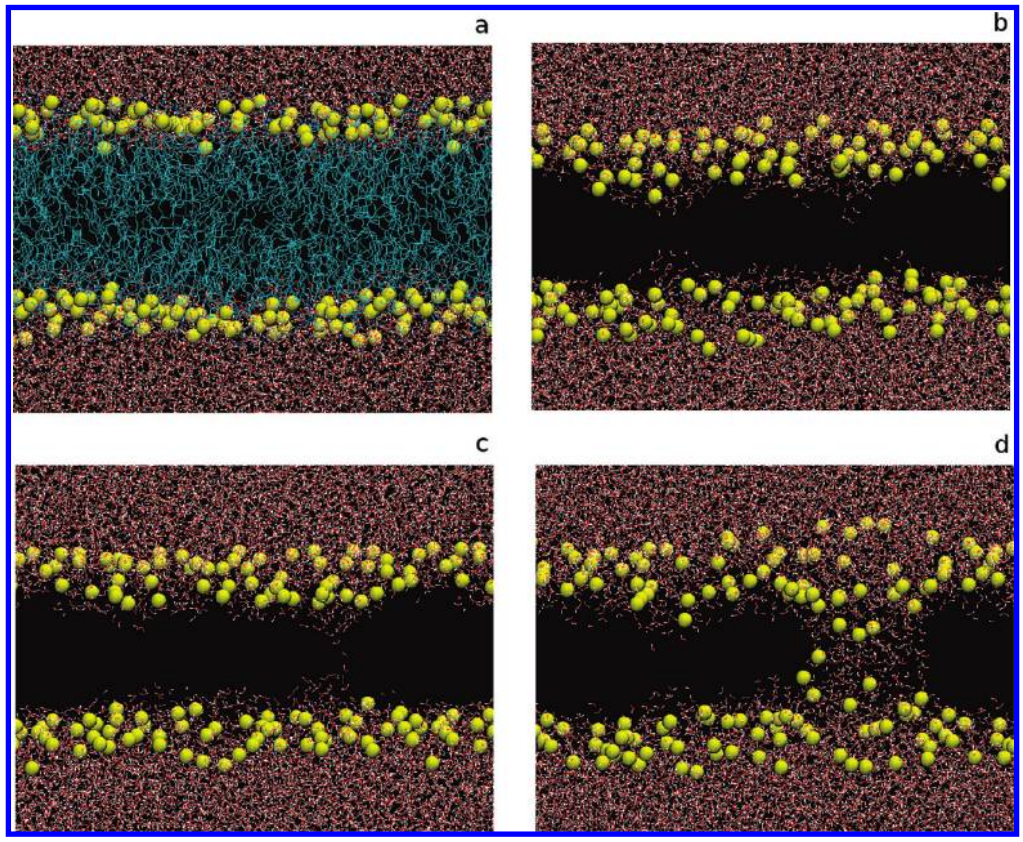

Figure 10. Snapshots for the pore dynamics in a DOPC bilayer subjected to an applied electric field $E_{ap} = E_0 = 325$ mV/nm (see also Figure 8): (a) initial configuration; (b) 9520 ps; (c) 9550 ps; (d) 9750 ps. Water molecules are plotted with red and white sticks; DOPC phosphate groups, with yellow beads. In the initial configuration, DOPC molecules are plotted using blue sticks. Periodic boundary conditions are applied in the *xy* plane.

the two leaflets takes a longer time of the order of a few nanoseconds (snapshots in Figures 11b and 11c are separated by almost 2 ns). Actually, it takes so long that when the hydrophobic pore is formed, some lipid head groups are already oriented to the pore in its cathodic side (see differences between Figures 10c and 11c). Finally, as shown in Figure 11d, cholesterol and DOPC molecules from both leaflets rotate to form the hydrophilic pore. Interestingly, cholesterol molecules, despite being less flexible than DOPC, take advantage of their deeper insertion into the membrane and rotate faster than DOPC molecules.

It is worth noticing that our simulations can be used for the determination of E_0 and the description of the mechanism of pore formation, which is the focus of this paper, but not for the study of fully developed steady pores. When the simulated membranes are electroporated, the MD trajectories show the complete sequence of pore formation. However, the formed pore grows, and in few nanoseconds reaches the size of the simulation box. The bilayers then collapse and different lyotropic phases in the "*xz*" and/or "*yz*" planes appear due to the effect of periodic boundary conditions. The study of stable pores cannot be therefore performed with such small bilayers, and it was attempted with larger membranes consisting of 6×6 replicates (4608 DOPC molecules). When these membranes became electroporated, the simultaneous generation and growth of several pores were observed. The study of these pores, however, is rather problematic because strong undulations appear soon after the electric field is applied. A close inspection of the membranes shows that the regions with higher curvature coincide with the growing pores, so that membrane deformation appears to be strongly coupled to pore growth and stability. This behavior has been previously found in large DOPC cholesterol-free membranes (2304 lipids) subjected to an external electric field.[13] The conclusion is that a different strategy has to be used to study steady pores in nearly flat membranes to avoid strong membrane deformations, so the analysis of the pore structure (size, stability, lipid organization, etc.) will correspond to a more realistic context. This study is beyond the scope of this paper and will be presented in a future publication.

4. Conclusions

The permeabilization of a lipid bilayer by applying a transverse electric field, a phenomenon called electroporation, is the basis of diverse medical techniques such as electrochemotherapy. Furthermore, cholesterol is a unique lipid component in biological membranes[51] and is known to determine most of their structural properties. As a consequence, it is clear that the effect of cholesterol in the bilayer electroporation process is fundamental for its technical application to natural cell membranes.

In this paper, MD simulations of DOPC bilayers with different contents of cholesterol have been performed, and for each case the electroporating field threshold E_0 has been calculated and the properties of the membrane have been analyzed. It has been found that the condensing action of cholesterol increases the cohesive nature of the host membrane, and as a consequence, cholesterol-containing membranes require a stronger electric field to be electroporated than the pure case. In particular, we found that membrane cohesion sharply increases at Chol contents above 10 mol %, in accordance to the sudden increment

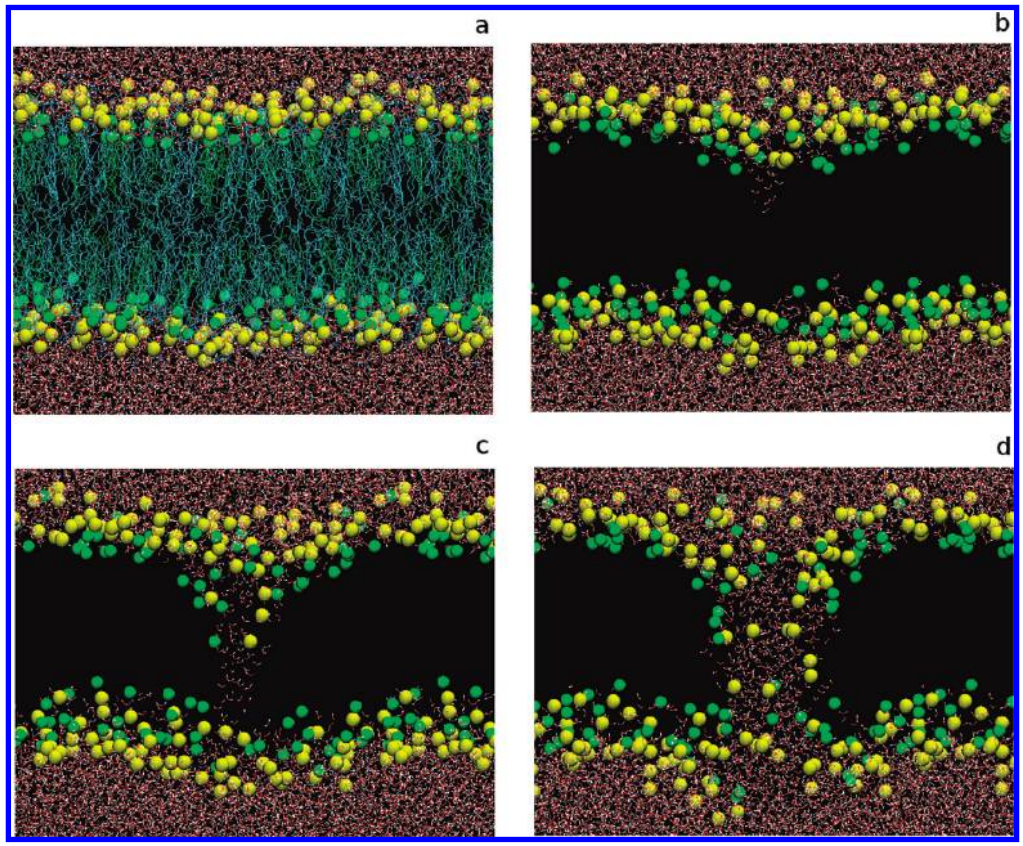

Figure 11. Snapshots for the pore dynamics in a DOPC bilayer with 40 mol % Chol, subjected to an applied electric field $E_{ap} = E_0 = 750$ mV/nm (see also Figure 9): (a) initial configuration; (b) 5850 ps; (c) 7800 ps; (d) 8850 ps. Water molecules are plotted with red and white sticks; DOPC phosphate groups and Chol hydroxyl groups, with yellow and green beads, respectively. In the initial configuration, DOPC and Chol molecules are plotted using blue and green sticks, respectively. Periodic boundary conditions are applied in the *xy* plane.

of E_0 above this Chol fraction. Thus, our model is able to capture not only the structural effects that cholesterol induces in equilibrium biological membranes but also those that show up when an external electric field is applied. The former are related to the behavior observed for the main structural bilayer parameters (area per molecule, bilayer thickness, chain ordering) and the latter correspond to the cohesive nature of the membrane and its sudden increase above 10 mol % Chol.

Several transverse profiles have been examined to study the behavior of the lipid/water interface when the electric field is applied. By means of these profiles we explain that some water molecules at the interface could become aligned with the applied field and nucleate a fluctuation that initiates a hole in the hydrophobic region of the membrane and may eventually progress as a pore. Such water defects are more likely found in the cathodic leaflet. The effect of headgroup dipoles is also examined, but it is not found to play a causative role in the electroporation process.

The complete sequence of pore formation has been analyzed. First, a water fluctuation penetrates the membrane and forms a very thin cone of water molecules. If this water filament progresses, it may eventually reach the anodic leaflet, forming a thin hydrophobic pore. After a while, the lipids around the pore rotate and cover the water filament with their hydrophilic head groups, forming a hydrophilic pore that rapidly widens. Although this sequence is common to all simulated systems, some distinct features are noticed between cholesterol-free and cholesterol-containing membranes. In the former case, the occurrence of water fluctuations is much higher and once a fluctuation sufficiently penetrates the membrane, the formation of the hydrophobic and hydrophilic pores is almost simultaneous. The hydrophobic pore only lasts a few hundreds of picoseconds since DOPC molecules quickly rotate to stabilize the pore. Instead, for cholesterol-containing membranes, the kinetics of pore formation is much slower. First, the fluctuations are less probable than for the pure case. Second, when a large enough fluctuation is formed, it takes more time (even a few nanoseconds) to traverse the membrane and connect the two leaflets. Third, once the hydrophobic pore has been formed, cholesterol and DOPC molecules rotate to form the hydrophilic pore. Interestingly, it has been observed that cholesterol molecules, despite being less flexible than DOPC, take advantage of their deeper insertion into the membrane and rotate faster than DOPC molecules once the hydrophobic pore has been formed.

Summarizing, we have contributed to a detailed understanding of the role of cholesterol in electroporation phenomenon. Our ultimate goal has been to obtain a better model to elucidate the molecular processes that occur during the application of the electric field to cells or biological tissues, and how one of the most important components of the cell membrane (cholesterol) can affect the electroporation process.

Acknowledgment. This work was carried out under partial financial support provided by SEID through the project FIS200603525 and by DURSI through the project 2009-SGR1055. Computational resources were provided by the Barcelona Supercomputing Center. M.L.F. and G.M. are researchers at the Consejo Nacional de Investigaciones Científicas y Técnicas (CONICET) and their work was partially supported by grants from Universidad de Buenos Aires (UBACyT X132/08), CONICET (PIP 5756/05), ANPCyT (PME 184/

04), and the Agencia Española de Cooperación Internacional (AECI A/8402/07). We thank Hector Martinez-Seara and Esteban Mocskos for his help in some computational and technical issues.

Supporting Information Available: Some simulations have been performed with the original GROMOS87 force field, showing that electric fields higher than for the improved force field used in this paper are required to porate the membrane. This material is available free of charge via the Internet at http://pubs.acs.org.

References and Notes

(1) Houslay, M. D.; Stanley, K. K. *Dynamics of Biological Membranes*; Wiley: New York, 1982.
(2) Sackmann, E. Biological membranes architecture and function. In *Structure and Dynamics of Membranes*; Lipowsky, R., Sackmann, E., Eds.; Elsevier: Amsterdam, 1995; pp 1−64.
(3) Tieleman, D. P.; Marrink, S. J. *J. Am. Chem. Soc.* **2006**, *128*, 12462–12467.
(4) Humphrey, W.; Dalke, A.; Schulten, K. *J. Mol. Graph.* **1996**, *14*, 33–38.
(5) Tsong, T. Y. *Biophys. J.* **1991**, *60*, 297–306.
(6) Neumann, E.; Kakorin, S.; Toensing, K. *Bioelectrochem. Bioenerg.* **1999**, *48*, 3–16.
(7) Mir, L.; Bureau, M. F.; Gehl, J.; Rangara, R.; Rouy, D.; Caillaud, J.-M.; Delaere, P.; Branellec, D.; Schwartz, B.; Scherman, D. *Proc. Natl. Acad. Sci. U.S.A.* **1999**, *96*, 4262–4267.
(8) Prausnitz, M. R.; Bose, V. G.; Langer, R.; Weaver, J. C. *Proc. Natl. Acad. Sci. U.S.A.* **1993**, *90*, 10504–10508.
(9) Tsong, T. Y. *Methods Enzymol.* **1987**, *149*, 248–259.
(10) Mir, L. M.; Orlowski, S. *The Basis of Electrochemotherapy in Electrochemotherapy, Electrogenetherapy and transdermal drug delivery: electrically mediated delivery of molecules to cells*; Jaroszeski, M. J., Heller, R., Gilbert, R., Eds.; Springer: Berlin, 2000; pp 99−117.
(11) Belehradek, M.; Domenge, C.; Luboinski, B.; Orlowski, S.; Belehradek, J.; Mir, L. M. *Cancer* **1993**, *72*, 3694–3700.
(12) Sersa, G.; Miklavcic, D.; Cemazar, M.; Rudolf, Z.; Pucihar, G.; Snoj, M. *Eur. J. Surg. Oncol.* **2008**, *34*, 232–240.
(13) Tieleman, D. P. *BMC Biochem.* **2004**, *5*, 10.
(14) Ziegler, M. J.; Vernier, P. T. *J. Phys. Chem.* **2008**, *112*, 13588–13596.
(15) Leontiadou, H.; Mark, A. E.; Marrink, S. J. *Biophys. J.* **2004**, *86*, 2156–2164.
(16) Tarek, M. *Biophys. J.* **2005**, *88*, 4045–4053.
(17) Böckmann, R. A.; de Groot, B. L.; Kakorin, S.; Neumann, E.; Grubmüller, H. *Biophys. J.* **2008**, *95*, 1837–1850.
(18) Vernier, P. T.; Ziegler, M. J.; Sun, Y.; Chang, W. V.; Gundersen, M. A.; Tieleman, D. P. *J. Am. Chem. Soc.* **2006**, *128*, 6288–6289.
(19) Ohvo-Rekilä, H.; Ramstedt, B.; Leppimäki, P.; Slotte, J. P. *Prog. Lipid Res.* **2002**, *41*, 66–97.
(20) Bloom, M.; Evans, E.; Mouritsen, O. G. *Q. Rev. Biophys.* **1991**, *24*, 293–397.
(21) Martinez-Seara, H.; Róg, T.; Karttunen, M.; Reigada, R.; Vattulainen, I. *J. Chem. Phys.* **2008**, *129*, 105103.
(22) Tieleman, D. P.; Bentz, J. *Biophys. J.* **2002**, *83*, 1501–1510.
(23) Bachar, M.; Brunelle, P.; Tieleman, D. P.; Rauk, A. *J. Phys. Chem. B* **2004**, *108*, 7170–7179.
(24) Martinez-Seara, H.; Róg, T.; Pasenkiewicz-Gierula, M.; Vattulainen, I.; Karttunen, M.; Reigada, R. *Biophys. J.* **2008**, *95*, 3295–3305.
(25) Lindahl, E.; Hess, B.; van der Spoel, D. *J. Mol. Model.* **2001**, *7*, 306–317.
(26) van der Spoel, D.; Lindahl, E.; Hess, B.; Groenhof, G.; Mark, A. E.; Berendsen, H. J. C. *J. Comput. Chem.* **2005**, *26*, 1701–1718.
(27) Berger, O.; Edholm, O.; Jahnig, F. *Biophys. J.* **1997**, *72*, 2002–2013.
(28) Tieleman, D. P.; Berendsen, H. J. C. *J. Chem. Phys.* **1996**, *105*, 4871–4880.
(29) Holtje, M.; Forster, T.; Brandt, B.; Engels, T.; von Rybinski, W.; Holtje, H.-D. *Biochim. Biophys. Acta* **2001**, *1511*, 156–167.
(30) Berendsen, H. J. C.; Postma, J. P. M.; van Gunsteren, W. F.; Hermans, J. Interaction models for water in relation to protein hydration. In *Intermolecular Forces*; Pullman, B., Ed.; Reidel: Dordrecht, The Netherlands, 1981.
(31) Berendsen, H. J. C.; Postma, J. P. M.; van Gunsteren, W. F.; DiNola, A.; Haak, J. R. *J. Chem. Phys.* **1984**, *81*, 3684–3690.
(32) Miyamoto, S.; Kollman, P. A. *J. Comput. Chem.* **1992**, *13*, 952–962.
(33) Hess, B.; Bekker, H.; Berendsen, H. J. C.; Fraaije, J. G. E. M. *J. Comput. Chem.* **1997**, *18*, 1463–1472.
(34) Essman, U.; Perera, L.; Berkowitz, M. L.; Darden, H. L. T.; Pedersen, L. G. *J. Chem. Phys.* **1995**, *103*, 8577–8592.
(35) Martinez-Seara, H.; Róg, T.; Pasenkiewicz-Gierula, M.; Vattulainen, I.; Karttunen, M.; Reigada, R. *J. Phys. Chem. B.* **2007**, *111*, 11162–11168.
(36) Martinez-Seara, H.; Róg, T.; Karttunen, M.; Vattulainen, I.; Reigada, R. *J. Phys. Chem. B* **2009**, *113*, 8347–8356.
(37) Humphrey, W.; Dalke, A.; Schulten, K. *J. Mol. Graph.* **1996**, *14*, 33–38. http://www.ks.uiuc.edu/Research/vmd/.
(38) Hofsäß, C.; Lindahl, E.; Edholm, O. *Biophys. J.* **2003**, *84*, 2192–2206.
(39) Edholm, O.; Nagle, J. F. *Biophys. J.* **2005**, *89*, 1827–1832.
(40) Davis, J. H. *Biochim. Biophys. Acta* **1983**, *737*, 117–171.
(41) Nagle, J. F.; Tristram-Nagle, S. *Biochim. Biophys. Acta* **2000**, *1469*, 159–195.
(42) Kucerka, N.; Tristram-Nagle, S.; Nagle, J. F. *J. Membr. Biol.* **2005**, *208*, 193–202.
(43) Needham, D.; Hochmuth, R. M. *Biophys. J.* **1989**, *55*, 1001–1009.
(44) Koronkiewicz, S.; Kalinowski, S. *Biochim. Biophys. Acta* **2004**, *1661*, 196–203.
(45) Bennet, W. F. D.; MacCallum, J. L.; Tieleman, D. P. *J. Am. Chem. Soc.* **2009**, *131*, 1972–1978.
(46) Hung, W.-C.; Lee, M.-T.; Chen, F.-Y.; Huang, H. W. *Biophys. J.* **2007**, *92*, 3960–3967.
(47) Graziani, Y.; Livne, A. *J. Membr. Biol.* **1972**, *7*, 275–284.
(48) Finkelstein, A.; Cass, A. *Nature* **1967**, *216*, 717–718.
(49) Crowley, J. M. *Biophys. J.* **1973**, *13*, 711–724.
(50) Evans, E.; Needham, D. *J. Phys. Chem.* **1987**, *91*, 4219–4228.
(51) Bloch, K. *Cholesterol: evolution of structure and function in Biochemistry of Lipids, Lipoproteins and Membranes*; Vance, D. E., Vance, J. E., Eds.; Elsevier: Amsterdam, 1991; pp 363−381.
(52) Czub, J.; Baginski, M. *Biophys. J.* **2006**, *90*, 2368–2382.
(53) Pandit, S. A.; Bostick, D.; Berkowitz, M. L. *Biophys. J.* **2004**, *86*, 1345–1356.
(54) Vernier, P. T.; Ziegler, M. J. *J. Phys. Chem. B* **2007**, *111*, 12993–12996.

JP911605B